Dhanyasi et al., http://www.jcb.org/cgi/content/full/jcb.201503005/DC1

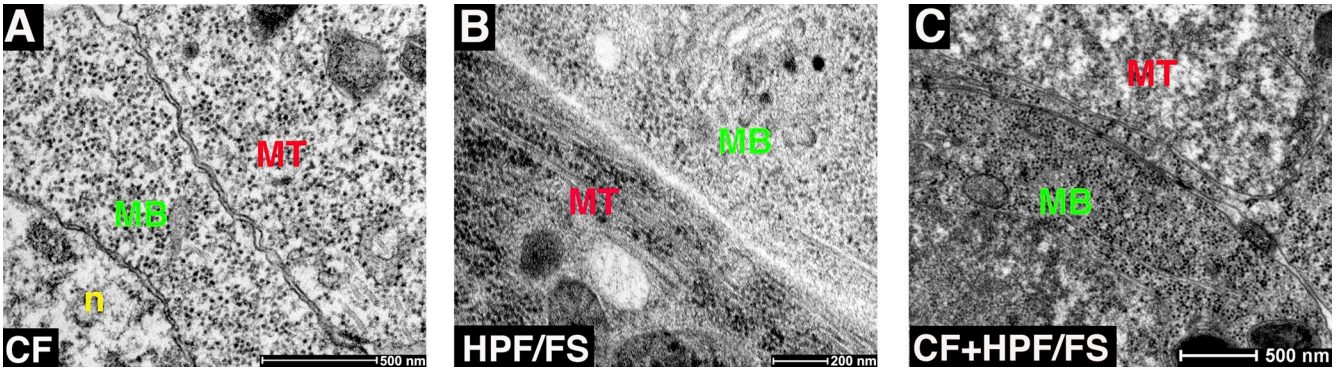

Figure S1. **A combined chemical/cryofixation protocol faithfully preserves myogenic cell features.** (A) A key consideration in studies of this kind is the choice of a proper TEM tissue processing protocol that will faithfully preserve cell structure and organization. In particular, we were concerned with our ability to preserve the outer plasma membranes of fusing cells so that the details of membrane fusion could be followed with confidence. Standard CF and ethanol/acetone dehydration protocols have been a longstanding method of choice for studies of this nature, but these relatively harsh approaches are known to distort and compromise the quality of membrane preparations (van Weering et al., 2010). Indeed, we found that IFM preparations dissected and processed in this manner often produce a prominent waviness in the appearance of the myoblast membranes and, furthermore, lose much of the cytoplasmic content of the cells. MT, myotube; MB, myoblast; n, nucleus. (B) HPF, followed by dehydration via FS, is considered a highly useful and far less artifact-prone alternative to CF (McDonald and Auer, 2006). One drawback to this approach, however, is an inherent difficulty in visualization of plasma and intracellular membranes, necessitating the development of various procedural modifications to the FS step (Walther and Ziegler, 2002; Giddings, 2003). In our hands as well, HPF/FS processing of pupal IFMs resulted in clearly superior preservation of cytoplasmic constituents, but cell membrane features were inconsistent and often difficult to observe altogether, limiting the usefulness of this procedure for our purposes. (C) To attempt to overcome these obstacles, we decided to use a hybrid protocol in which HPF cryofixation is preceded by an aldehyde fixation step (Sosinsky et al., 2008). Originally developed and used as a means for properly preserving sensitive nerve tissue before HPF, this method has produced excellent TEM visualization of cellular membranes in diverse samples and applications, including electron tomography of budding viral particles (Welsch et al., 2010), electron tomography of cardiac muscle excitation-contraction machinery (Hayashi et al., 2009), and TEM-level analysis of the murine visual system (Möbius et al., 2010). Indeed, application of the CF/HPF procedure to pupal IFM preparations resulted in TEM images showing a high degree of cytoplasm preservation, coupled with a strikingly clear demarcation of continuous and smooth cell membranes (also see Fig. 1, E and E'). This protocol was therefore judged to be particularly appropriate for our purposes and was used throughout the study.

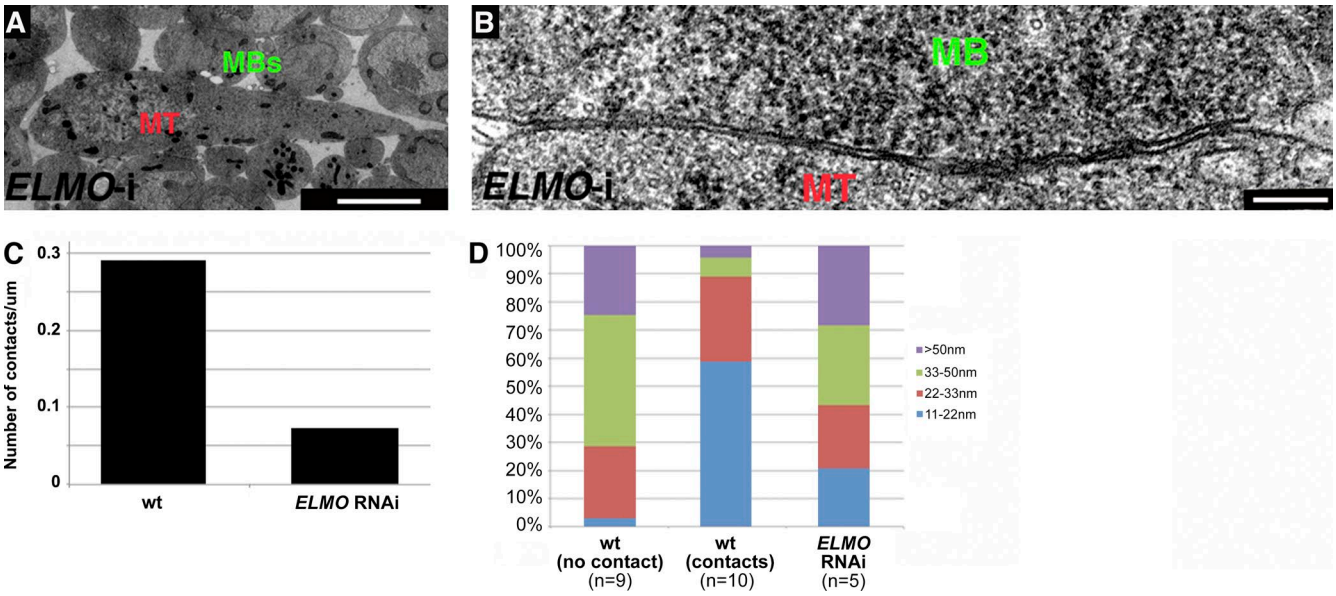

Figure S2. **Features of DLM fusion arrest after knockdown of *ELMO*.** (A and B) DLMs after knockdown of *ELMO* (also referred to as *CED-12*), which encodes the *Drosophila* homologue of a conserved bipartite Rac-GEF. (A) A low magnification view demonstrates the resulting strong fusion arrest phenotype, with myoblasts (MBs) congregating around a thin myotube (MT). (B) High magnification view reveals the relatively wide gap between an *ELMO* knockdown myotube (MT) and a neighboring myoblast (MB) and the absence of any cell–cell contacts. The myoblast does not flatten its myotube-apposed surface. (C) Bar graph demonstrating the low frequency of contact sites along apposed myotube–myoblast surfaces after knockdown of *ELMO*. The number of cell pairs examined and the total length of membrane surveyed for contact sites in the different genotypes were as follows. WT: 50 cell pairs, ~200 µm; and *ELMO* knockdown: 14 cell pairs, ~40 µm. (D) Bar graph comparing the distribution of myoblast–myotube intermembrane distances. *ELMO* knockdown DLMs display a distance distribution profile in which ~50% of membrane separations are of intermediate value (22–50 nm). A similar profile is characteristic of WT DLM preparations where the cells do not make contact (left bar). Panels should be compared with the data shown in Fig. 3. Bars: (A) 2 µm; (B) 200 nm. wt, wild type.

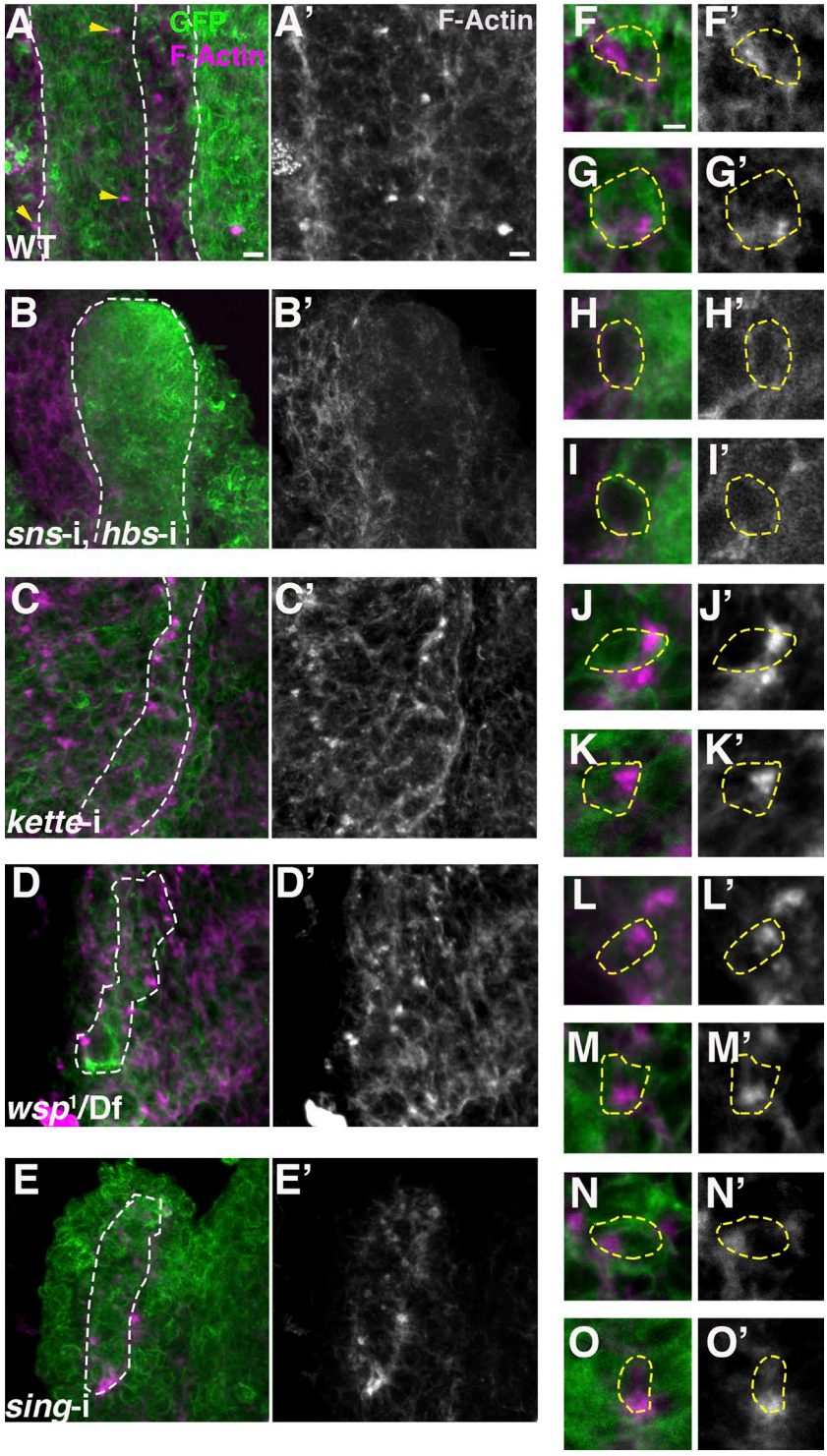

Figure S3. **Features of the fusion-associated F-actin foci that form at the DLM myoblast–myotube interface in different genetic backgrounds.** DLM preparations from pupae of different genetic backgrounds at 20 h APF. All pupae harbored *mef2*-GAL4 and UAS-*mCD8-GFP* transgenes for visualization of myogenic tissue and the relevant UAS-RNAi constructs where required. Pupae were stained with anti-GFP antibodies (green) and phalloidin-Atto647 (magenta and gray) for visualization of F-actin structures. The two left columns show low magnification views with single myotubes outlined. Note the reduced size of the various mutant myotubes. Arrows in A point to typical WT actin foci. The two right columns show high magnification views of myoblast–myotube interfaces. Myoblast contours are outlined. WT DLMs (A and A′, F and F′, and G and G′) show transient, round actin foci that form and dismantle at the time of fusion. Foci do not form altogether in *sns/hbs* knockdown DLMs (B and B′, H and H′, and I and I′). Numerous foci are found in fusion-arrested *kette* knockdown (C and C′, J and J′, and K and K′), *wsp*^{1} hemizygote (D and D′, L and L′, and M and M′), and *sing* knockdown (E and E′, N and N′, and O and O′) DLMs. The foci in the *kette* knockdown DLMs are enlarged and misshapen, whereas the foci in *wsp*^{1} hemizygote and *sing* knockdown DLMs resemble WT foci. Bars: (A and A′) 5 µm; (F) 2 µm.

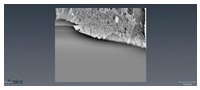

Video 1. **FIB/SEM visualization of a WT IFM myotube and surrounding myoblasts.** IFMs were dissected from pupae (20 h APF) and processed for serial view imaging as described in Materials and methods section FIB/SEM imaging. The video shows consecutive views of the sample surface, as it is milled (in steps of 10 nm) by the ion beam. The images comprising the dataset were segmented using the paintbrush tool of the AMIRA 3D visualization software. The myotube is false-colored light green, and the myoblasts are individually colored in the resulting 3D reconstruction. The display rate is 20 frames/s.

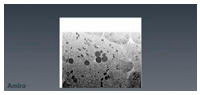

Video 2. **FIB/SEM visualization of a *WASp* mutant IFM myotube (*wsp*^{1}/Df(3R)3450) and surrounding myoblasts (20 h APF).** Data collection and image processing were performed as in Video 1. The myotube is false-colored light green, and the myoblasts are individually colored in the resulting 3D reconstruction. Note the presence of myoblast extensions. The display rate is 20 frames/s.

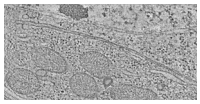

Video 3. **Tomogram of a portion of the interface between a WT IFM myotube and a closely apposed myoblast, demonstrating the coexistence of cell contacts and small fusion pores.** IFMs were dissected from pupae (20 h APF) and processed as for conventional TEM (described in Materials and methods section TEM). STEM was performed on 350–400-nm-thick sections. Images were collected for every 1.5° tilt angle from 70° to −70°. Images were aligned using gold fiducial markers in IMOD. Segmentation, rendering, and 3D visualization were performed using AVIZO 3D visualization software. Transient red arrows point to examples of contact sites that were used for the 3D reconstruction. In the reconstruction, contact sites are colored green, membrane discontinuities (pores) are colored yellow, and the plasma membranes are colored pink. The display rate is 37 frames/s.

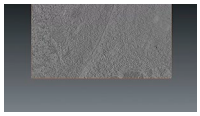

Video 4. **Tomogram of a single pore.** Data collection and image processing were performed as in Video 3. Transient red arrow points to the pore used for the 3D reconstruction, where the pore is colored yellow and the plasma membranes are colored pink. The display rate is 22.5 frames/s.

References

Giddings, T.H. 2003. Freeze-substitution protocols for improved visualization of membranes in high-pressure frozen samples. *J. Microsc.* 212:53–61. http://dx.doi.org/10.1046/j.1365-2818.2003.01228.x

Hayashi, T., M.E. Martone, Z. Yu, A. Thor, M. Doi, M.J. Holst, M.H. Ellisman, and M. Hoshijima. 2009. Three-dimensional electron microscopy reveals new details of membrane systems for Ca^{2+} signaling in the heart. *J. Cell Sci.* 122:1005–1013. http://dx.doi.org/10.1242/jcs.028175

McDonald, K.L., and M. Auer. 2006. High-pressure freezing, cellular tomography, and structural cell biology. *Biotechniques.* 41:137–143: 139: 141 passim. http://dx.doi.org/10.2144/000112226

Möbius, W., B. Cooper, W.A. Kaufmann, C. Imig, T. Ruhwedel, N. Snaidero, A.S. Saab, and F. Varoqueaux. 2010. Electron microscopy of the mouse central nervous system. *In* Methods in Cell Biology. Vol. 96. T. Müller-Reichert, editor. Elsevier. 475–512.

Sosinsky, G.E., J. Crum, Y.Z. Jones, J. Lanman, B. Smarr, M. Terada, M.E. Martone, T.J. Deerinck, J.E. Johnson, and M.H. Ellisman. 2008. The combination of chemical fixation procedures with high pressure freezing and freeze substitution preserves highly labile tissue ultrastructure for electron tomography applications. *J. Struct. Biol.* 161:359–371. http://dx.doi.org/10.1016/j.jsb.2007.09.002

van Weering, J.R.T., E. Brown, T.H. Sharp, J. Mantell, P.J. Cullen, and P. Verkade. 2010. Intracellular membrane traffic at high resolution in electron microscopy of model systems. *In* Methods in Cell Biology. Vol. 96. T. Müller-Reichert, editor. Elsevier. 619–648.

Walther, P., and A. Ziegler. 2002. Freeze substitution of high-pressure frozen samples: the visibility of biological membranes is improved when the substitution medium contains water. *J. Microsc.* 208:3–10. http://dx.doi.org/10.1046/j.1365-2818.2002.01064.x

Welsch, S., L. Kolesnikova, V. Krähling, J.D. Riches, S. Becker, and J.A. Briggs. 2010. Electron tomography reveals the steps in filovirus budding. *PLoS Pathog.* 6:e1000875. http://dx.doi.org/10.1371/journal.ppat.1000875